JACS
JOURNAL OF THE AMERICAN CHEMICAL SOCIETY
Article
pubs.acs.org/JACS

High-Pressure Synthesis of 5d Cubic Perovskite $BaOsO_3$ at 17 GPa: Ferromagnetic Evolution over 3d to 5d Series

Youguo Shi,[†,‡,⬡] Yanfeng Guo,*[,†,⬡,★] Yuichi Shirako,[§,⬠] Wei Yi,[∥] Xia Wang,[†] Alexei A. Belik,[∥] Yoshitaka Matsushita,[⊥] Hai Luke Feng,[†,#] Yoshihiro Tsujimoto,[▽] Masao Arai,[♦] Nanlin Wang,[‡] Masaki Akaogi,[§] and Kazunari Yamaura*[,†,#]

[†]Superconducting Properties Unit, National Institute for Materials Science, 1-1 Namiki, Tsukuba, Ibaraki 305-0044, Japan
[‡]Institute of Physics, Chinese Academy of Sciences, P.O. Box 603, Beijing 100190, China
[§]Department of Chemistry, Gakushuin University, 1-5-1 Mejiro, Toshima-ku, Tokyo 171-8588, Japan
[∥]International Center for Materials Nanoarchitectonics (WPI-MANA), National Institute for Materials Science, 1-1 Namiki, Tsukuba, Ibaraki 305-0044, Japan
[⊥]Materials Analysis Station, National Institute for Materials Science, 1-2-1 Sengen, Tsukuba, Ibaraki 305-0047, Japan
[#]Graduate School of Chemical Sciences and Engineering, Hokkaido University, North 10 West 8, Kita-ku, Sapporo, Hokkaido 060-0810, Japan
[▽]Materials Processing Unit, National Institute for Materials Science, 1-2-1 Sengen, Tsukuba, Ibaraki 305-0047, Japan
[♦]Computational Materials Science Unit, National Institute for Materials Science, 1-1 Namiki, Tsukuba, Ibaraki 305-0044, Japan

Supporting Information

ABSTRACT: In continuation of the series of perovskite oxides that includes $3d^4$ cubic $BaFeO_3$ and $4d^4$ cubic $BaRuO_3$, $5d^4$ cubic $BaOsO_3$ was synthesized by a solid-state reaction at a pressure of 17 GPa, and its crystal structure was investigated by synchrotron powder X-ray diffraction measurements. In addition, its magnetic susceptibility, electrical resistivity, and specific heat were measured over temperatures ranging from 2 to 400 K. The results establish a series of d^4 cubic perovskite oxides, which can help in the mapping of the itinerant ferromagnetism that is free from any complication from local lattice distortions for transitions from the 3d orbital to the 5d orbital. Such a perovskite series has never been synthesized at any d configuration to date. Although cubic $BaOsO_3$ did not exhibit long-range ferromagnetic order unlike cubic $BaFeO_3$ and $BaRuO_3$, enhanced feature of paramagnetism was detected with weak temperature dependence. Orthorhombic $CaOsO_3$ and $SrOsO_3$ show similar magnetic behaviors. $CaOsO_3$ is not as conducting as $SrOsO_3$ and $BaOsO_3$, presumably due to impact of tilting of octahedra on the width of the t_{2g} band. These results elucidate the evolution of the magnetism of perovskite oxides not only in the 5d system but also in group 8 of the periodic table.

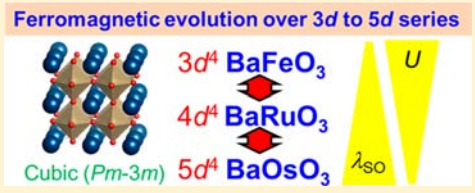

INTRODUCTION

Transition metal oxides, which are electronically and magnetically active, are emerging as functional materials for a broad range of scientific and practical applications owing to their high-temperature superconductivity, multiferroicity, metal−insulator transitions, and spintronics.[1−9] Transition metal oxides that exhibit a variety of solid states have been fabricated; however, the electronic properties of these oxides are extraordinarily rich, and hence it has been challenging to map out even their primary magnetic properties, given the limited number of material parameters available. Establishing a series of transition metal oxides that can aid in the mapping of the properties of these materials would be a significant step in comprehensively understanding the chemistry of not only solid-state transition metal oxides but also nanoscaled magnetic and electronic oxides as well as other materials.

Recent studies of transition metal oxides have focused on perovskite-based 5d oxides since the properties of the correlated 5d electrons seem to be fundamentally different from those of the electrons of 3d oxides[1−4] such as iron, manganese, and copper oxides,[5−9] which have been widely used in various applications. The major differences in the electromagnetic properties of 3d and 5d oxides are primarily caused by the fact that the 5d orbital is spatially more extended than the 3d orbital. This strengthens the hybridization between the 5d and oxygen 2p orbitals. In addition, the spin−orbit (SO) interaction of the 5d atoms is stronger than that of the 3d atoms because the SO coupling is roughly proportional to the fourth power of the effective nuclear charge (atomic number).[10,11] Indeed, a delicate balance between the nearly comparable magnitudes (~0.5−2 eV)[1−4] of the on-site Coulomb repulsion, U, and the bandwidth, W, and the magnitude of the SO interaction in 5d perovskite-based oxides

Received: July 19, 2013
Published: October 3, 2013

dx.doi.org/10.1021/ja4074408 | J. Am. Chem. Soc. 2013, 135, 16507−16516

may drive distinguishable phenomena such as the unconventional insulating state of Sr_2IrO_4 ($5d^4$)[1−4] and the Slater-like transition of $NaOsO_3$ ($5d^3$).[12−15] To the best of our knowledge, the SO coupling constant for even free 3d and 5d ions has not yet been experimentally determined.[11] Therefore, an experimental evaluation of the nature of d electrons for orbitals ranging from 3d to 5d would be significant for further developing perovskite-based 5d oxides that are fundamentally different from 3d oxides.

In this study, we focused our attention on a perovskite-based 5d oxide, namely, $5d^4$ $BaOsO_3$. The large crystal field of a 5d atom usually stabilizes the low-spin (LS) configuration; thus, $5d^0$ and $5d^6$ oxides do not have unpaired 5d electrons, exhibiting only a nonmagnetic state. Perovskite-based $5d^1$ and $5d^2$ oxides, such as Re^{5+},[16] Re^{6+},[17] and Os^{6+}[18] oxides, are rare. In addition, their synthesis is usually very challenging. Several $5d^4$ and $5d^5$ oxides as well as $5d^3$ oxides have been synthesized and characterized.[1−4,19−21] Unlike $5d^4$ and $5d^5$ oxides, $5d^3$ oxides exhibit a minor SO interaction owing to their configuration.[12−15,22] We therefore focused our attention on the $5d^4$ and $5d^5$ electrons. In practice, a number of perovskite-based d^4 and d^5 oxides, which cover 3d to 5d orbitals, have been synthesized. These include Sr_2TrO_4 (d^4 Tr = Fe^{4+},[23] Ru^{4+};[24] d^5 Tr = Co^{4+},[25] Rh^{4+},[26] Ir^{4+1-4}) and $SrTrO_3$ (d^4 Tr = Fe^{4+},[27] Ru^{4+},[28] Os^{4+};[29,30] d^5 Tr = Co^{4+},[31] Rh^{4+},[32] Ir^{4+}.[33]) However, in these oxides, octahedral TrO_6 distortion and tilting seem to have a significant effect on the features of the d electrons, as was suggested for the Sr and Ca series of oxides.[27−30] Very recently, cubic $3d^4$ $BaFeO_3$[34] and cubic $4d^4$ $BaRuO_3$[35] were synthesized, establishing a new distortion-free perovskite series. Both these cubic perovskite oxides have the same space group, $Pm\bar{3}m$, with all the atoms located at special positions: Ba(0, 0, 0), Tr(1/2, 1/2, 1/2), and O(1/2, 1/2, 0). Therefore, if cubic $5d^4$ $BaOsO_3$ is added to the series, the nature of the d electrons should be known for 3d to 5d orbitals without there being significant influence from a local lattice distortion.

In this study, we were able to synthesize cubic $5d^4$ $BaOsO_3$ to complete the series of d^4 perovskite oxides that includes $3d^4$ cubic $BaFeO_3$ and $4d^4$ cubic $BaRuO_3$ by a solid-state reaction at a pressure of 17 GPa. The results of crystal structure investigations through X-ray diffraction (XRD) analyses indicated that the space group of the oxide was the same as that of $BaFeO_3$ and $BaRuO_3$, namely $Pm\bar{3}m$. This series of cubic perovskite oxides with valence orbitals ranging from 3d to 5d can aid in the mapping of the evolution of d^4 magnetism that is free from complications from local lattice distortions. Such a textbook-like perovskite series has never been synthesized for any group of the periodic table.

EXPERIMENTAL PROCEDURES

Polycrystalline $CaOsO_3$, $SrOsO_3$, and $BaOsO_3$ were synthesized by a solid-state reaction under high-pressure and high-temperature conditions. Polycrystalline $CaOsO_3$ and $SrOsO_3$ were synthesized in a belt-type high-pressure apparatus operated at the National Institute for Materials Science, Japan. This apparatus could maintain a pressure of 6 GPa during the heating stage. The starting materials were fine powders of CaO, SrO, and OsO_2 (Os-84.0%, Alfa Aesar). The CaO and SrO precursors were obtained by firing $CaCO_3$ (99.99%, Kojundo Chemical Lab. Co.) at 1000 °C for 10 h in air and $SrCO_3$ (99.9%, Kojundo Chemical Lab. Co.) at 1100 °C for 24 h in air, respectively. A mixture of the powders was sealed in a Pt capsule in a glovebox filled with Ar. The reaction temperatures at 6 GPa were 1700 and 1500 °C for $CaOsO_3$ and $SrOsO_3$, respectively. After being heated for 1 h, the capsule was quenched to room temperature, and the pressure within was reduced.

Cubic $BaOsO_3$ was prepared using a two-step process. First, polycrystalline $BaOsO_3$, which crystallizes into a 6H hexagonal structure,[29,30] was synthesized by heating a stoichiometric mixture of BaO_2 (95%, Sigma-Aldrich), OsO_2, and Os (99.9%, Alfa Aesar) at 1700 °C for 1 h in the same high-pressure apparatus . Next, a powder of 6H $BaOsO_3$ was placed into a smaller Pt capsule and heated in a Kawai-type multianvil high-pressure apparatus operated at Gakushuin University, Japan.[36] The reaction conditions were a temperature of 1600 °C, a reaction time of 30 min, and a pressure of 17 GPa. The capsule was then quenched to room temperature, and the pressure within was released.

The three polycrystalline compounds, $CaOsO_3$, $SrOsO_3$, and $BaOsO_3$, were studied through powder XRD analyses, which were performed at room temperature using monochromatic Cu Kα radiation, to confirm the quality of the compounds. A Rigaku diffractometer was employed for the purpose. To investigate the crystal structures of the compounds in detail, the compounds were studied through synchrotron powder XRD (SXRD) measurements at room temperature, which were performed using a large Debye−Scherer camera at the BL15XU beamline of SPring-8, Japan.[37,38] The wavelength of the monochromatic radiation was 0.65297 Å, determined using a standard material. The obtained SXRD patterns were analyzed by the Rietveld method using the software programs RIETAN-FP[39] and VESTA.[40]

The temperature dependence of the electrical resistivity, $\rho(T)$, of the materials was measured between 2 and 400 K by the four-probe method using a physical properties measurement system from Quantum Design, Inc. Electrical contacts were formed on a bar-shaped pellet, cut out from each final product, using silver paste and Au wires. The gauge current was 0.1 or 0.2 mA. The specific heats (C_p) were measured using the same apparatus and a relaxation-time method over temperatures ranging from 2 to 300 K. The direct current (DC) magnetic susceptibility (χ) was measured in the zero-field cooling (ZFC) and field cooling (FC) modes over temperatures ranging from 2 to 400 K. A magnetic property measurement system from Quantum Design, Inc., was used for the measurements. The applied magnetic field was 50 kOe. The isothermal magnetization $M(H)$ at 2 and 300 K was measured using the same apparatus for magnetic fields ranging from −50 to 50 kOe. A loosely ground powder of each compound was used for the magnetic measurements.

The electronic states of the perovskites $CaOsO_3$, $SrOsO_3$, and $BaOsO_3$ were studied by a first-principles method. The electronic densities of states (DOS) of the compounds were calculated by the generalized gradient approximation (GGA) method,[41] which is based on the density functional theory.[41] The WIEN2K software package, which is based on the highly precise full-potential linearized augmented-plane-wave method, was used for the calculations.[42]

RESULTS

The synthesis of perovskite compounds with the $5d^4$ configuration, $CaOsO_3$, $SrOsO_3$, and $BaOsO_3$, under ambient-pressure and high-pressure conditions (pressure of up to 6.5 GPa) was reported by Chamberland et al. in 1973[29] and 1978.[30] The compounds $CaOsO_3$ and $SrOsO_3$ crystallize into an orthorhombic $GdFeO_3$-type structure with the space group *Pnma*, while $BaOsO_3$ crystallizes into the six-layer hexagonal (6H) $BaTiO_3$ structure. In addition, $BaOsO_3$ crystallizes into a body-centered cubic polymorph with a lattice parameter of 9.373(1) Å, which was reported to be a $KSbO_3$-type compound.[30] The cubic perovskite $BaOsO_3$ had not been synthesized previously.

In the present study, the synthesis of the orthorhombic perovskites $CaOsO_3$ and $SrOsO_3$ was performed, and the structure and electromagnetic properties of these compounds were studied. Although their properties have been investigated to some extent in earlier works, a detailed study was lacking. In

dx.doi.org/10.1021/ja4074408 | J. Am. Chem. Soc. 2013, 135, 16507−16516

addition, we found that 6H $BaOsO_3$ transforms into a cubic polymorph on heating at 17 GPa. As a result, a new series of the cubic perovskite d^4 $BaTrO_3$ (Tr = Fe^{4+},[34] Ru^{4+},[35] and Os^{4+} [this work]) was established. This series could be useful for studying the evolution of the electromagnetic properties of perovskites over a transition from the 3d orbital to the 5d orbital because the cubic structure is free from local lattice distortions that often have an effect on electromagnetic properties. The cubic perovskite series could help in the mapping of the fundamental d^4 properties for a transition from the 3d orbital to the 5d orbital. Such a cubic perovskite series has never been available to date, not only in the d^4 configuration but also in other d configurations.

First, the crystal structure of $BaOsO_3$ was studied by SXRD analysis. Figure 1 shows a refined SXRD pattern of reasonable

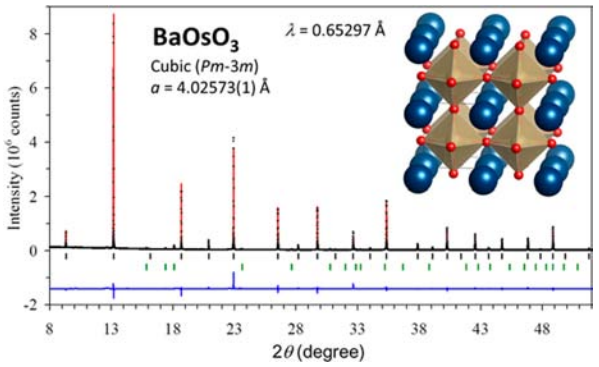

Figure 1. Observed (crosses) and calculated (solid line) synchrotron X-ray powder diffraction patterns of BaO_sO_3 at room temperature, as well as the differences between them. The small markers at the bottom denote the simulated peak positions. The lower marks are for an impurity phase, which is 2.9 wt % Os. Inset shows the structure inferred after refinement.

quality of $BaOsO_3$. A cubic perovskite structure model was used to refine the pattern. The *R* factors of the refinement were lower than 5.8%, indicating a reasonable quality.[39] The crystal picture drawn from the refined solution is shown in Figure 1. As a result of the refinement, the possibility of the formation of a $KSbO_3$-type polymorph could be rejected. In addition, a trivial amount of impurity was detected; this was presumably Os with the weight fraction of 2.9%. Details of the refinement are listed in Table 1. We emphasize that the refinement of occupation factors of the Ba and Os sites gave values equal to the unity within standard deviations.

Structures of $SrOsO_3$ and $CaOsO_3$ could be refined in the $GdFeO_3$-type model with space group *Pnma*. While a reasonable structural model was obtained for $CaOsO_3$, the OsO_6 octahedron was highly distorted in $SrOsO_3$. The careful

Table 1. Structural Parameters of Cubic $BaOsO_3$ at Room Temperature[a]

site	WP	*x*	*y*	*z*	*B* (Å^2)
Ba	1*a*	0	0	0	0.272(8)
Os	1*b*	0.5	0.5	0.5	0.032(6)
O	3*c*	0.5	0.5	0	0.37(6)

[a]WP, Wyckoff position. The occupancy factor was fixed at 1 for all atoms. The space group is $Pm\bar{3}m$ (No. 221). $Z = 1$, $a = 4.02573(1)$ Å, and $V = 65.2430(1)$ Å^3. The *R* indexes were $R_{wp} = 5.79\%$, $R_p = 3.68\%$, $R_B = 5.54\%$, and $R_F = 3.77\%$.

analysis of the SXRD pattern of $SrOsO_3$ showed that reflections with intensities above 0.2% could be index in space group *Imma* with the same lattice parameters. The refinement in the *Imma* model gave similar *R* indexes ($R_{wp} = 3.33\%$, $R_p = 1.83\%$, $R_B = 3.74\%$, and $R_F = 2.30\%$) in comparison with the *Pnma* model ($R_{wp} = 3.31\%$, $R_p = 1.80\%$, $R_B = 3.76\%$, and $R_F = 2.60\%$). The tilt system of *Imma* is $a^0b^-b^-$ while that of *Pnma* is $a^+b^-b^-$.[43,44] Therefore, the appearance of extremely weak superstructure reflections (<0.2%) could originate from additional octahedral tilt along the "pseudo-cubic" *a* axis. Extremely weak superstructure reflections originating from ordering of oxygen atoms and the presence of heavy Sr and Os cations could prevent accurate localization of the O2 atom in the *Pnma* model. Therefore, we used constraints, $z(O2) = 1 - x(O2)$ and $B(O2) = B(O1)$, during the refinement of $SrOsO_3$ in the *Pnma* model. The refined structural parameters for $SrOsO_3$ and $CaOsO_3$ are listed in Tables 2 and 3, respectively. The lattice parameters of

Table 2. Structural Parameters of Orthorhombic $SrOsO_3$ at Room Temperature[a]

site	WP	*x*	*y*	*z*	*B* (Å^2)
Sr	4*c*	0.0115(5)	0.25	0.9945(6)	1.483(15)
Os	4*b*	0	0	0.5	0.560(5)
O1	4*c*	0.500(4)	0.25	0.0443(12)	1.55(9)
O2	8*d*	0.257(3)	0.0219(10)	0.743	1.55

[a]The occupancy factor was fixed at 1 for all atoms. The space group is *Pnma* (No. 62). $Z = 4$, $a = 5.55925(1)$ Å, $b = 7.88779(2)$ Å, $c = 5.59802(1)$ Å, and $V = 245.4745(9)$ Å^3. The *R* indexes were $R_{wp} = 3.31\%$, $R_p = 1.80\%$, $R_B = 3.76\%$, and $R_F = 2.60\%$.

Table 3. Structural Parameters of Orthorhombic $CaOsO_3$ at Room Temperature[a]

site	WP	*x*	*y*	*z*	*B* (Å^2)
Ca	4*c*	−0.0491(2)	0.25	0.9906(8)	0.64(3)
Os	4*b*	0	0	0.5	0.47(1)
O1	4*c*	0.5272(12)	0.25	0.0855(7)	0.49(11)
O2	8*d*	0.2128(7)	0.0460(4)	0.7970(7)	0.59(9)

[a]The occupancy factor was fixed at 1 for all atoms. The space group is *Pnma* (No. 62). $Z = 4$, $a = 5.57439(3)$ Å, $b = 7.77067(4)$, $c = 5.44525(3)$ Å, and $V = 235.871(2)$ Å^3. The *R* indexes were $R_{wp} = 3.14\%$, $R_p = 2.03\%$, $R_B = 1.76\%$, and $R_F = 1.83\%$.

$SrOsO_3$ and $CaOsO_3$ are comparable to those reported previously.[29,30] Figures 2 and 3 show the refinement fits. We emphasize that the (110) cubic reflection was split into three strong reflections in $SrOsO_3$, thus excluding tetragonal and rhombohedral symmetries. All reflections of $SrOsO_3$ could only be indexed in an orthorhombic symmetry with the reported lattice parameters. We also emphasize that in $SrOsO_3$, the *a* parameter is smaller than the *c* parameter ($a < b/\sqrt{2} < c$) for both *Imma* and *Pnma* models in comparison with $CaOsO_3$ ($c < b/\sqrt{2} < a$). Exchange of the *a* and *c* parameters in $SrOsO_3$ gave similar refinement results, but expected positions of a few very weak reflections did not match with the experimental positions, thus confirming the order of the lattice parameters. The same order of the lattice parameters was observed in $SrRuO_3$ and $SrIrO_3$ ($a < b/\sqrt{2} < c$). Note that sometimes the *a* and *c* parameters of $SrRuO_3$ and $SrIrO_3$ were erroeneously exchanged in the literature.

Small amounts of impurities (Os in $SrOsO_3$ and Os and $Ca_2Os_2O_7$ in $CaOsO_3$) were detected in $SrOsO_3$ and $CaOsO_3$.

dx.doi.org/10.1021/ja4074408 | J. Am. Chem. Soc. 2013, 135, 16507−16516

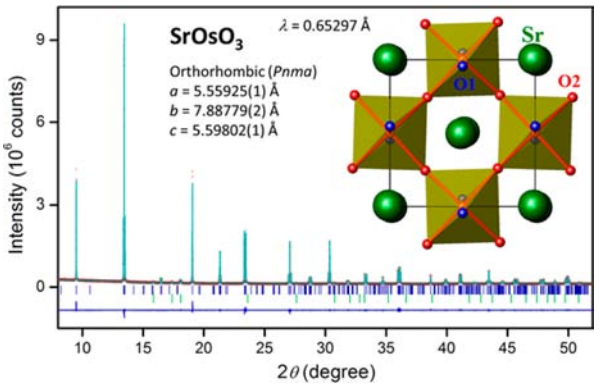

Figure 2. Observed (crosses) and calculated (solid line) synchrotron X-ray powder diffraction patterns of $SrOsO_3$ at room temperature in the *Pnma* model, as well as the differences between them. The small markers at the bottom denote the simulated peak positions. The lower marks are for an impurity phase, which is 1.95 wt % Os. Inset shows the structure projection along the *b* axis.

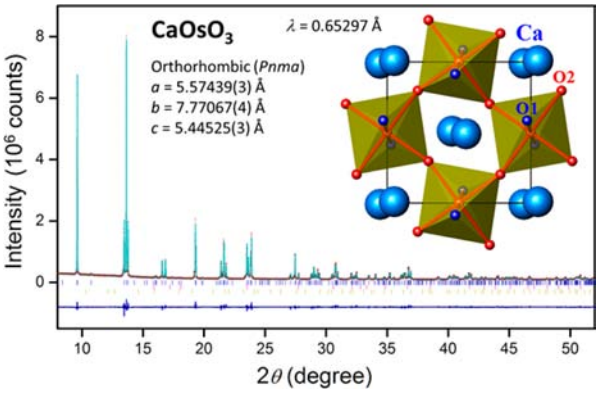

Figure 3. Observed (crosses) and calculated (solid line) synchrotron X-ray powder diffraction patterns of $CaOsO_3$ at room temperature, as well as the differences between them. The small markers at the bottom denote the simulated peak positions. The middle and lower marks are for impurity phases, which are 0.37 wt % Os and 0.07 mass % $Ca_2Os_2O_7$, respectively. Inset shows the structure inferred after refinement.

It is worth noting that Os is paramagnetic at temperatures as low as 0.66 K and eventually becomes superconductive.[45] Thus, the presence of small amounts of Os by mass fraction should have a negligible impact on electromagnetic characterization at temperatures greater than 2 K. In addition, the mass fraction of $Ca_2Os_2O_7$ in the Ca-based compound was ~0.07%, suggesting that the impurity had little impact on the measurements, although it does drive a metal−insulator transition at 327 K.[46]

In the $AOsO_3$ series (A = Ca, Sr, and Ba), the decrease of the size of the A cations results in the appearance of additional tilting and the increase of tilt angles to adjust for smaller A cations while keeping almost rigid and regular OsO_6 octahedra. $BaOsO_3$ has ideal OsO_6 octahedra without tilts (the tilt system is $a^0a^0a^0$, and the Os−O−Os bond angles are 180°). $SrOsO_3$ adopts basically the $a^0b^-b^-$ tilt system (the inset of Figure 2, with negligible tilt along the *Pnma b* axis), and the Os−O−Os bond angles are 165.7° and 169.5°. $CaOsO_3$ has the $a^+b^-b^-$ tilt system (the inset of Figure 3, with noticeable tilt along the *Pnma b* axis), and the Os−O−Os bond angles are 151.7° and 152.0°. The tilt angles can be estimated from the fractional coordinates of the O1 and O2 atoms and the lattice parameters: in-phase tilt angle $\phi_{O2} = \arctan(1 + 2x_{O2} - 2z_{O2})$, out-of-phase tilt angles $\varphi_{O2} = \arctan(2^{5/2}y_{O2})$ and $\varphi_{O1} = \arctan(2^{3/2}z_{O1})$ [for our coordinates in space group *Pnma*], and $\phi_{lattice} = \arccos[\sqrt{2}c^2/(ab)]$ for $c < b/\sqrt{2} < a$.[47] Values of φ_{O2}, φ_{O1}, and $\phi_{lattice}$ were very close to each other for $CaOsO_3$ and $SrOsO_3$ (Table 4) indicating that the OsO_6 octahedra were very rigid. It is interesting that ϕ_{O2} was just 1.7° in $SrOsO_3$ in comparison with $SrRuO_3$ (ϕ_{O2} = 5.9°) and $CaOsO_3$ (ϕ_{O2} = 9.6°) (see Table S1, Supporting Information).

The local structure distortion was evaluated on the basis of the bond valence sums (BVSs, where BVS = $\sum_{i=1}^{N} v_i$, $v_i = \exp[(R_0 - l_i)/B]$, N is the coordination number, B = 0.37, $R_0(Os^{4+})$ = 1.811, $R_0(Fe^{4+})$ = 1.780, and $R_0(Ba^{2+})$ = 2.29), which are listed in Table 4.[48] The BVSs for the Ba atoms in $BaOsO_3$, $BaRuO_3$, and $BaFeO_3$ are far greater than the expected value of 2.00.[48] The high degree of overbonding suggests the presence of significant internal stress. In addition, the tolerance factor is slightly higher than 1.00, even though $BaOsO_3$, $BaRuO_3$, and $BaFeO_3$ all have a cubic perovskite lattice.[51] These results thus suggest that the internal bonds of $BaOsO_3$, $BaRuO_3$, and $BaFeO_3$ are under certain stresses, which may account for the extreme conditions required to synthesize the compounds.

Table 4. Comparison of the Lattice and Structural Parameters of the Perovskite Oxides

	$CaOsO_3$	$SrOsO_3$	$BaOsO_3$	$BaRuO_3$[49]	$BaFeO_3$[50]
space group	*Pnma*	*Pnma*	$Pm\bar{3}m$	$Pm\bar{3}m$	$Pm\bar{3}m$
a (Å)	5.57439(3)	5.55925(1)	4.02573(1)	4.0059(2)	3.97106(1)
b (Å)	7.77067(4)	7.88779(2)			
c (Å)	5.44525(3)	5.59802(1)			
d_{calcd} (g/cm^3)	7.836	8.817	9.558	7.398	6.230
Tr−O1 (Å)	2.003(1) × 2	1.9875(9)	2.0129(1) × 6	2.0029(1)	1.9856(1)
Tr−O2 (Å)	1.978(4) × 2	1.9803(9)			
Tr−O2 (Å)	2.037(4) × 2	1.9811(9)			
Tr−O1−Tr (deg)	151.7(1) × 2	165.7(1)	180	180	180
Tr−O2−Tr (deg)	152.0(2) × 4	169.5(2)			
BVS at A-site	1.90 (^{VIII}), 2.04 (^{XII})	2.09 (^{xII})	2.63 (^{xII})	2.73 (^{xII})	2.92 (^{xII})
BVS at B-site	3.55	3.77	3.48	3.80	3.44
tolerance factor *t*	0.95	0.99	1.05	1.05	1.07
ϕ_{O2} (deg)	9.6	1.7			
φ_{O2}, φ_{O1}, $\phi_{lattice}$ (deg)	14.6, 13.6, 14.5	7.1, 7.1, 8.2			

dx.doi.org/10.1021/ja4074408 | J. Am. Chem. Soc. 2013, 135, 16507−16516

The BVSs for Sr and Os in $SrOsO_3$ are nearly comparable with the expected values. In addition, the tolerance factor is close to 1.00.[51] But $SrOsO_3$ has an orthorhombic distortion similar to $SrRuO_3$, which also has $t \approx 1.00$. Because this type of octahedral distortion usually has a large impact on the correlated d electrons, it is essential to carefully investigate the magnetic and electrical properties of the $CaOsO_3$, $SrOsO_3$, and $BaOsO_3$.

All the compounds exhibited negligible thermal hysteresis in the $\rho(T)$ curves on warming and cooling over temperatures ranging from 2 to 400 K (Figure 4). $CaOsO_3$ showed

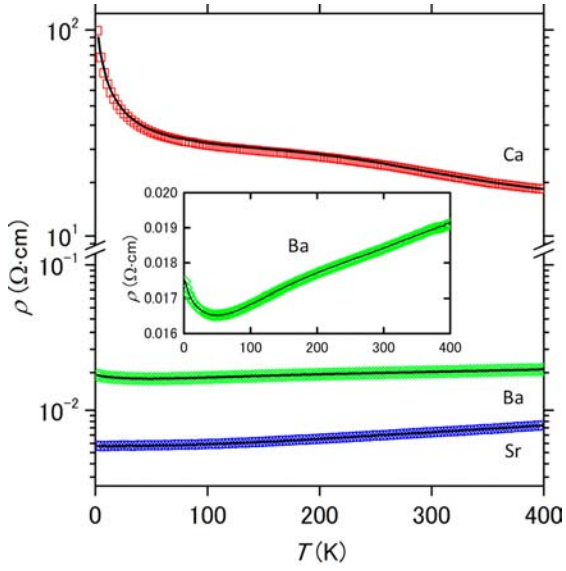

Figure 4. Temperature dependence of ρ of $AOsO_3$ (A = Ba, Sr, and Ca). Inset: an expanded view of the $\rho(T)$ data for $BaOsO_3$.

semiconductor-like $\rho(T)$ values (i.e., $d\rho/dT < 0$) over the entire temperature range. The ρ value at room temperature was ~16.9 Ω cm, which was approximately 3 orders of magnitude or more higher than what is expected for a metallic oxide.[52] On cooling, ρ increased gradually to 28 Ω cm at 80 K and 102 Ω cm at 2 K. However, neither the Arrhenius conduction model [$\ln \rho(T) \propto T^{-1}$] nor the variable range hopping [$\ln \rho(T) \propto T^{-1/4}$] one[53] fits the $\rho(T)$ values for $CaOsO_3$. Thus, the semiconductor-like behavior is possibly affected by the complex scattering, which involves grain boundaries and undetected disorder. A simple explanation could be that $CaOsO_3$ is in the vicinity of a Mott insulating regime, as has been hypothesized in the case of Sr_2IrO_4.[1−4] Further studies involving a high-quality single crystal are required to fully characterize the $\rho(T)$ behavior of $CaOsO_3$.

In contrast to $CaOsO_3$, $SrOsO_3$ remained metallic until the lowest temperature (2 K). The value of ρ at room temperature was 7.85 mΩ cm, and it decreased gradually upon cooling to 5.66 mΩ cm at 2 K. The $\rho(T)$ curve for temperatures lower than 250 K followed the power law relation, $\rho(T) = \rho_0 + A_0T^2$, to a high degree. This relation is usually indicative of Fermi liquid-like behavior when ρ_0 and A_0 are constant. A least-squares analysis yielded ρ_0 = 5.67 mΩ cm and A_0 = 0.796 mΩ cm K^{-2}. The ρ_0 value was unusually larger than that for a normal metal,[8] suggesting additional scattering by the grain boundaries and undetected disorders, for instance. In addition, the residual resistivity ratio, ρ_{300}/ρ_0, was 1.24; this was much smaller than what is expected for a metallic material.[28]

The $\rho(T)$ curve for $BaOsO_3$ showed a broad upturn at a temperature of approximately 60 K; the conductivity of the compound changed from metal-like to non-metal-like upon cooling. Note that this change was not accompanied by thermal hysteresis, indicating that a first-order phase transition was unlikely. Regardless of the change, $\rho(T)$ remained very low over the entire temperature range, suggesting that the charged-carrier density was altered little over the upturn. Analyzing the metallic conduction behavior using the formula for Fermi liquids yielded ρ_0 = 17.43 mΩ cm and A_0 = 0.441 mΩ cm K^{-2}. The ρ_0 value was approximately three times larger than that of $SrOsO_3$, suggesting that additional scattering at such as grain boundaries might be significant. Indeed, the nonmetallic behavior for temperatures lower than approximately 30 K followed well the variable-range hopping model, indicating that disorder scattering has greater impact on the conduction at the low temperatures. Alternatively, a possible pseudogap nature is responsible for the weak upturn, as was argued for similar features observed for $SrIrO_3$ and 9R-$BaRuO_3$.[49] The delicate transport issue needs to be investigated using a single crystal $BaOsO_3$.

The temperature dependence of χ was measured for all the compounds, as shown in Figure 5a. It was found that the

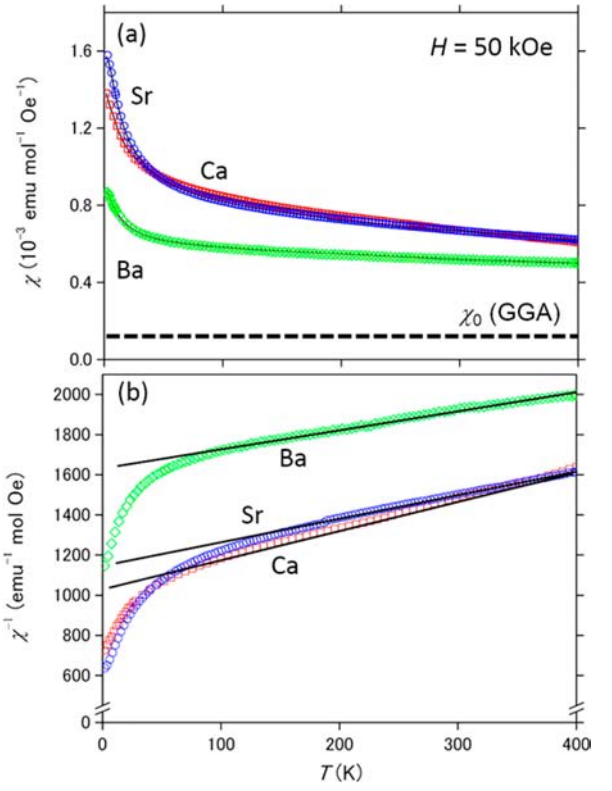

Figure 5. (a) Temperature dependence of χ for $AOsO_3$, measured at 50 kOe during cooling (A = Ba, Sr, and Ca) and (b) a χ^{-1} vs T plot of the data. The solid lines denote the least-squares fits to the data.

temperature did not have a significant effect on χ, unlike a localized spin system. In addition, a long-range ferromagnetic order as found for cubic $BaRuO_3$ and $BaFeO_3$ were not obvious above 2 K. This was true for all the compounds and the entire temperature range. Although a small rise in χ upon cooling at low temperatures was observed, magnetic ordering accompanied by the metallic to nonmetallic change at approximately 60 K was not, unlike in the case of $NaOsO_3$.[12]

dx.doi.org/10.1021/ja4074408 | J. Am. Chem. Soc. 2013, 135, 16507−16516

Table 5. Comparison of the Curie–Weiss and C_p Parameters of the Perovskite Oxides

parameter	$CaOsO_3$	$SrOsO_3$	$BaOsO_3$
Curie–Weiss Parameters without χ_0			
μ_{eff} (μ_B)	2.302(4)	2.659(1)	3.037(7)
C (emu mol^{-1} Oe^{-1} K)	0.663(2)	0.884(1)	1.153(5)
Θ_W (K)	−682(3)	−1028(1)	−1911(9)
χ_0 (emu mol^{-1} Oe^{-1})	0 (fixed)	0 (fixed)	0 (fixed)
Curie–Weiss Parameters with χ_0			
μ_{eff} (μ_B)	0.685(6)	0.586(2)	0.403(1)
C (emu mol^{-1} Oe^{-1} K)	0.0586(9)	0.0429(3)	0.0203(1)
Θ_W (K)	0 (fixed)	0 (fixed)	0 (fixed)
χ_0 (10^{-4} emu mol^{-1} Oe^{-1})	4.74(4)	5.18(1)	4.51(3)
C_p Parameters			
γ (mJ mol^{-1} K^{-2})	18.1(1)	27.3(2)	16.8(1)
β (10^{-4} J mol^{-1} K^{-4})	2.15(1)	0.98(4)	2.19(2)
T_D (low temp) (K)	355.2(7)	462(6)	353(1)
T_D (K)	692(7)	712(10)	710(13)
n_D	3.83(3)	2.89(3)	3.25(4)
T_E (K)	170(2)	172(2)	173(3)
n_E	1.75(4)	1.78(4)	2.24(6)
Theoretically Expected Values with the SO Interaction			
χ_0 (10^{-4} emu mol^{-1} Oe^{-1})	1.23	1.42	1.16
γ (mJ mol^{-1} K^{-2})	8.1	9.3	7.6

To quantitatively analyze the magnetic properties of the compounds, the $1/\chi$ vs T plots of all the compounds were fit to the Curie–Weiss (CW) law; these are the solid curves in Figure 5b. The analytical formula used was $\chi = N_A\mu_{eff}^2/[3k_B(T - \Theta_W) + \chi_0]$, where N_A is the Avogadro constant, μ_{eff} is the effective Bohr magneton, k_B is the Boltzmann's constant, Θ_W is the Weiss temperature, and χ_0 is the temperature-independent term. When we assumed that $\chi_0 = 0$, a least-squares fit of the data for temperatures greater than 200 K yielded Θ_W = −1911(9) K and μ_{eff} = 3.037(7) μ_B for $BaOsO_3$, Θ_W = −1028(1) K and μ_{eff} = 2.659(1) μ_B for $SrOsO_3$, and Θ_W = −682(3) K and μ_{eff} = 2.302(4) μ_B for $CaOsO_3$. It appeared that the values of the magnetic parameters Θ_W and μ_{eff} for $BaOsO_3$ were greater than those for $CaOsO_3$. Note that the spin-only value for $S = 1$ (Os^{4+}, t_{2g}^4) gave a μ_{eff} [$= 2(S(S + 1))^{1/2}$] of 2.83 μ_B, which was slightly lower than that observed for $BaOsO_3$ and slightly higher than those for $SrOsO_3$ and $CaOsO_3$. Note that similar μ_{eff} of ∼2.6 μ_B was observed for a series of $Sr_{1-x}Ba_xRuO_3$.[49] In contrast, when we assumed $\Theta_W = 0$, a not insignificant χ_0 was obtained by the least-squares fit, indicating possible enhanced paramagnetism. Indeed, the observed χ_0 was approximately 3.6–3.9 times larger than the Pauli paramagnetism estimated theoretically by first-principles calculations (Table 5).

The above results were achieved on the extreme assumptions either with or without χ_0. The true magnetic parameters are probably between the two sets of the parameters. We have, however, technical difficulties in estimation of χ_0 by analysis of the χ data; the available temperature range was too narrow to reasonably establish the parameters. If we extend the temperature range in the χ measurements far beyond 400 K, it could be helpful in the estimation; however, the heating may increase risk from osmium tetroxide exposure. Thus, we did not conduct the high-temperature χ measurements for $AOsO_3$.

In practice, itinerant features were observed in the transport measurements for all $AOsO_3$ (A = Ba, Sr, and Ca; note that specific data shown later indicated that $CaOsO_3$ has itinerant electrons). Therefore, contribution of itinerant electrons should be carefully evaluated to correctly analyze the observed magnetism. It should be kept in mind, however, that the applicability of the Curie–Weiss law to an itinerant system such as cubic $BaOsO_3$ is not justified theoretically, although in practice one can obtain useful results. Thus, we report the analysis results for future reference. In addition, SO interactions might have an impact on 5d magnetism,[11] a quantitative analysis that takes into account theoretical considerations should be attempted. The values of the magnetic parameters for $AOsO_3$ are listed in Table 5.

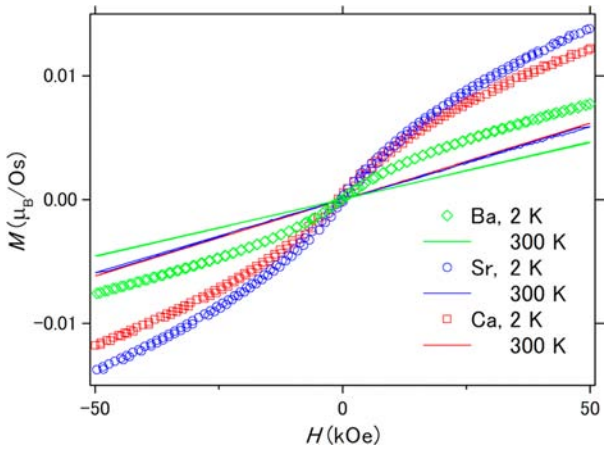

Figure 6. Isothermal magnetization at 2 and 300 K for $AOsO_3$ (A = Ba, Sr, and Ca).

To investigate the magnetic properties of the compounds further, the isothermal magnetization of the compounds was measured at 2 and 300 K, as shown in Figure 6. The measured magnetization curves indicated that the compounds did not exhibit a significant degree of magnetization upon cooling. In addition, magnetic hysteresis was not obvious in any of the curves; therefore no long-range magnetic order was established over the temperature and composition ranges investigated. The curvature of the magnetization curves at 2 K for the compounds may reflect the nature of the possible enhanced paramagnetism and magnetic impurity contributions. Further analysis is left for future study.

Figure 7 shows a comparison of the total DOS for electronic states around the Fermi energies (E_F) of $BaOsO_3$, $SrOsO_3$, and $CaOsO_3$, estimated by taking into consideration the SO interaction in the first-principles calculations. In all compounds, the E_F level is located very near the peak structure, suggesting the presence of magnetic instabilities. As stated previously, the 5d orbital is spatially more extended than the 3d orbital, strengthening hybridization between the 5d and oxygen 2p orbitals. The high degree of hybridization in 5d oxides, which is greater than that in 3d and 4d oxides, significantly broadens the DOS structure around the E_F level in general. In addition, the 5d t_{2g} band is slightly broadened from the Ca to Ba compositions; $CaOsO_3$ is not as conducting as $SrOsO_3$ and $BaOsO_3$, presumably due to the impact of tilting of octahedra on the width of the t_{2g} band as can be seen in Figure 7a. Although strong hybridization is generally not conducive to magnetic instabilities, the observed χ_0 was approximately 3.6–3.9 times larger than the Pauli paramagnetic susceptibilities estimated theoretically from the total DOS at E_F for the Ca to Ba compositions. The enhanced χ_0 of the cubic perovskite $BaOsO_3$ might indicate proximity to itinerant ferromagnetism.

dx.doi.org/10.1021/ja4074408 | J. Am. Chem. Soc. 2013, 135, 16507–16516

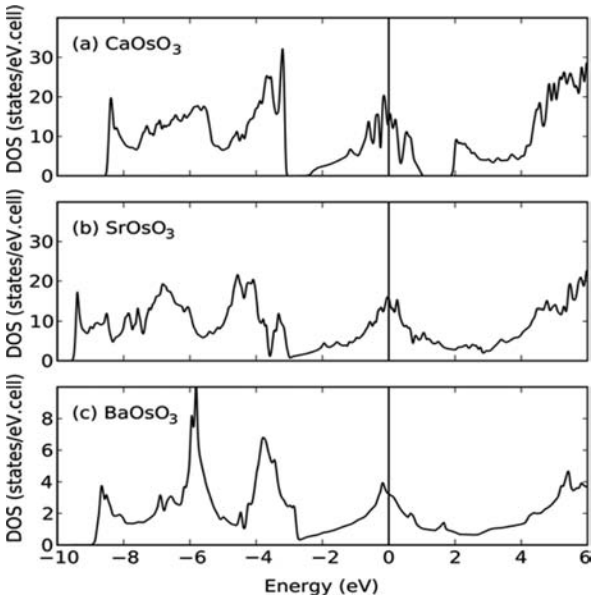

Figure 7. Total DOS for (a) $CaOsO_3$, (b) $SrOsO_3$, and (c) $BaOsO_3$.

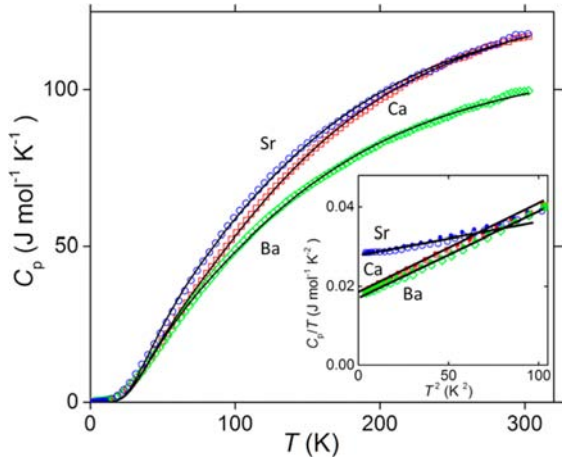

Figure 8. $C_p(T)$ of $AOsO_3$ (A = Ba, Sr, and Ca). Inset shows the C_p/T vs T^2 plots for the compounds at low temperatures. The solid line and curve denote the least-squares fits to the data.

Note that the first-principles calculations mentioned above employed experimentally determined crystal structure parameters. In addition, we also tested the theoretically optimized crystal structure parameters; however only trivial changes were noticed.

To further characterize the magnetic behavior of the compounds, the C_p values of the compounds were measured, as shown in Figure 8. $C_p(T)$ changed rather monotonically to 2 K, showing that no major phase transitions took place in this temperature range. The plots of C_p vs T were quantitatively analyzed using a linear combination of the Debye model and the Einstein model. The analytical formula used was

$$C_p(T) = n_D \times 9N_A k_B \left(\frac{T}{T_D}\right)^3 \int_0^{T_D/T} \frac{x^4 e^x}{(e^x - 1)^2}\, dx + n_E \times 3N_A k_B \left(\frac{T_E}{T}\right)^2 \frac{e^{T_E/T}}{(e^{T_E/T} - 1)^2}$$

where N_A is Avogadro's constant and T_D and T_E are the Debye and Einstein temperatures, respectively. The scale factors, n_D and n_E, corresponded to the number of vibrational modes per formula unit in the Debye and Einstein models, respectively. Fitting the curves yielded a T_D of 710(13) K, T_E of 173(3) K, n_D of 3.25(4), and n_E of 2.24(6) for $BaOsO_3$; the values for $SrOsO_3$ and $CaOsO_3$ were very similar (these are listed in Table 5). The Einstein term, which was linearly added to the Debye term, dramatically increased the quality of the fit in all the cases, suggesting that the phonon DOS at frequencies corresponding to 300 K or lower resulted in a much more complex DOS structure than that for the Debye model for all the compounds.

The inset shows an alternative plot of the data in the form of $C_p(T)/T$ vs T^2. The plots for all the compounds are displayed together for comparison. The linear trend of the plots indicates that the Debye approximation may characterize the temperature dependence of C_p for low temperatures. The least-squares analysis using the formula $C_p/T = \beta T^2 + \gamma$, where β and γ are a constant and the Sommerfeld coefficient, respectively, yielded $\beta = 2.19(2) \times 10^{-4}$ J mol^{-1} K^{-4} and $\gamma = 16.8(1)$ mJ mol^{-1} K^{-2} for $BaOsO_3$; $\beta = 0.98(4) \times 10^{-4}$ J mol^{-1} K^{-4} and $\gamma = 27.3(2)$ mJ mol^{-1} K^{-2} for $SrOsO_3$; and $\beta = 2.15(1)$ J mol^{-1} K^{-4} and $\gamma = 18.1(1)$ mJ mol^{-1} K^{-2} for $CaOsO_3$. The values of T_D calculated from the β values are listed in Table 5. Although ρ in the case of $CaOsO_3$ does not show a metallic temperature dependence, the γ value of 18.06 mJ mol^{-1} K^{-2} is substantially high and so are those for $BaOsO_3$ and $SrOsO_3$, implying the presence of a nontrivial electronic DOS at the E_F level. This disagreement suggests that the nonmetallic conduction of $CaOsO_3$ is possibly due to scattering by disorder including polycrystalline nature such as grain boundaries. The γ value of $SrOsO_3$ is approximately 1.5 times higher than those of $BaOsO_3$ and $CaOsO_3$; this may account for the fact that ρ for $SrOsO_3$ is the lowest over the entire temperature range.

The observed γ values were compared with the theoretically determined ones (Table 5). The comparison clearly indicated that the observed values were approximately 2.2 (Ca), 2.9 (Sr), and 2.2 (Ba) times greater than their theoretically determined counterparts. This increase is likely coupled with the enhanced magnetic susceptibility of the compounds and suggests that a magnetic instability in the compounds has an impact on their bulk properties. In addition, the γ increase is indeed present in cubic $BaOsO_3$. This proves that the octahedral distortion does not have a significant effect on the increase in γ.

DISCUSSION AND CONCLUSIONS

Previously, body-centered cubic $KSbO_3$-type $BaOsO_3$ with a lattice parameter of 9.373(1) Å had been synthesized under ambient pressure;[29,30] the calculated crystal density, d_{calcd}, had been 9.088 g cm^{-3}. In this study, we were able to successfully synthesize cubic $BaOsO_3$ perovskite. Synthesis via heating under high pressure (6−6.5 GPa) resulted in 6H $BaOsO_3$. Note that the previously reported lattice parameters for $BaOsO_3$ of a = 10.031(2) Å and c = 4.632(1) Å (d_{calcd} = 9.270 g/cm^3) indicate a two-layer hexagonal (2H) structure than a 6H one.[29,30] In general, a series of transitions are caused in the perovskite structure with a change in density;[54] each transition leads to a gain in crystal density in compounds such as $BaIrO_3$,[54] $BaRuO_3$,[49] and $BaFeO_3$.[50] In the present study, three-layer cubic (3C) $BaOsO_3$ was achieved at a d_{calcd} of 9.557 g cm^{-3}, confirming a part of the common sequence $KSbO_3$-type

dx.doi.org/10.1021/ja4074408 | J. Am. Chem. Soc. 2013, 135, 16507−16516

→ 2H → 9R → 4H → 6H → 3C, with the total gain in d_{calcd} being 5.2%.

In stark contrast to $CaOsO_3$ and $SrOsO_3$, $BaOsO_3$ has an ideal perovskite structure that is free of OsO_6 octahedral distortions and the buckling of the octahedral connections. In $CaOsO_3$ and $SrOsO_3$, the longer Os−O bonds in each octahedron are slightly longer than the shortest bonds (3.0% and <1%, respectively). On the other hand, in $BaOsO_3$, all Os−O bonds are of equal length. The bond angles for the interoctahedral Os−O−Os bonds are ∼152° and ∼165−170° for $CaOsO_3$ and $SrOsO_3$, respectively, whereas it is 180° for $BaOsO_3$. This variation in the bonds and tilts usually results in a significant difference in the magnetic and electrical properties, as has been found in the case of the compounds $ARuO_3$ and $AFeO_3$, where A = Ca and Sr.[34,35,55] For example, $CaRuO_3$ is metallic with increased paramagnetism for temperatures as low as 30 mK,[56] while $SrRuO_3$ is a ferromagnetic metal at temperatures lower than its Curie temperature (160 K). $AFeO_3$ compounds also exhibit complex magnetic behaviors, which are argued to be related to the degrees of freedom of the 3d spin, charge, and orbital in the locally distorted lattice. Thus, cubic $BaOsO_3$ is crucial for studying the evolution of the basic properties of d electrons for transitions from the 3d orbital to the 5d orbital in the absence of the influence of the local lattice distortion.

Figure 9 shows the magnetic-transition temperatures and crystal structures of the $3d^4$, $4d^4$, and $5d^4$ perovskite oxides; an

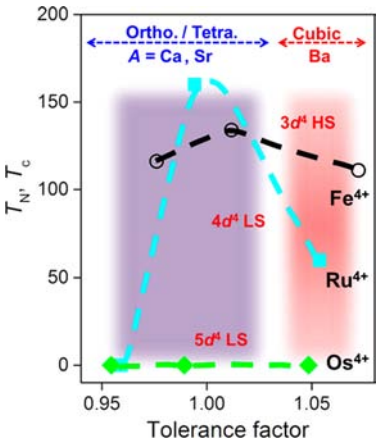

Figure 9. Magnetic transitions and tolerance factors of the d^4 perovskite oxides $ATrO_3$ (A = Ca, Sr, and Ba; Tr = Fe,[50] Ru,[57] and Os). T_c of $ARuO_3$ peaks out at tolerance factor of 1.[57]

outline of the magnetic evolution of the perovskite lattice can be seen in the figure. Unlike cubic $BaFeO_3$ and $BaRuO_3$, cubic $BaOsO_3$ may not satisfy the Stoner criterion for ferromagnetism, $D(E_F)I > 1$, where $D(E_F)$ is the DOS at E_F and I is the strength of the electron correlation. It is likely that the significantly radially extended 5d valence orbitals reduce $D(E_F)$ further, crossing the criterion. Although the degree of change of I for the transition from 3d to 5d is not known, the transition from the ferromagnetic high-spin (HS) state for $BaFeO_3$ to the paramagnetic LS state for $BaOsO_3$ via the ferromagnetic LS state for $BaRuO_3$ seems to be qualitatively consistent with the radially extended orbitals. Further theoretical considerations that take into account the I, U, and W values of the d^4 perovskite oxides are needed to be able to correctly characterize the ferromagnetic transition taking place between the 4d and 5d orbitals.

Generally, each d atom in a perovskite oxide is coordinated by six oxygen atoms, and the crystal field splits the d levels into lower t_{2g} and higher e_g levels with a $10D_q$ break. The $10D_q$ energy, which is normally ∼1 eV for $3d^4$ and >3 eV for $4d^4$ and $5d^4$,[58,59] can be increased by physically squeezing the crystal. Indeed, the HS state of $CaFeO_3$ transforms into the LS state on the application of a pressure of ∼30 GPa,[60] indicating that the $10D_q$ energy is greater than the magnitude of the Hund's coupling under this condition. Cubic $BaFeO_3$, however, may not exhibit a comparable spin-state transition within an experimentally feasible pressure range.[34] Therefore, a comparison of the magnetic and electrical properties of the LS configuration of cubic $BaFeO_3$ with those of cubic $BaRuO_3$ and $BaOsO_3$ has never been made.

In cubic $BaFeO_3$, the SO interaction is negligible.[10] Thus, the total angular momentum, J, can be approximated by the total spin angular momentum, S, which is equal to 2. Indeed, the ordered magnetic moment of 3.5 μ_B per Fe is close to the expected value of 4 μ_B for $S = 2$.[50] While cubic $BaRuO_3$ undergoes a ferromagnetic transition at 60 K with an ordered magnetic moment of 0.8 μ_B per Ru,[49] the moment is however far below the expected spin-only moment of 2 μ_B per Ru (t_{2g}^4 e_g^0), implying that S does not approximate J well. The interaction between the total orbital angular momentum, L, and S (LS coupling) or that between the individual angular momentums, j and j (jj coupling), has a nontrivial effect on the magnetism.

The SO interaction should increase for a move from 3d to 5d,[11] although a quantitative estimation of the same is yet to be performed. When the SO interaction is significant in a cubic perovskite, the degenerated 3 t_{2g} states should split into energetically lower 4 $J_{eff} = 3/2$ states and higher 2 $J_{eff} = 1/2$ states.[1−4] In this situation, the $J_{eff} = 3/2$ band is filled by d^4 electrons, resulting in the appearance of an electrically insulating state. However, cubic $BaOsO_3$ does not show such insulating behavior and is thus inconsistent with the J_{eff} picture. The strong disagreement suggests that an intermediate state between the jj coupling and the LS coupling is much closer to the true state of cubic $BaOsO_3$.[22] The ρ vs T curve for $BaOsO_3$ (inset of Figure 4) shows a broad upturn in the low-temperature region; this can be assumed to indicate that, over these temperatures, $BaOsO_3$ is in the vicinity of the metal-to-insulator boundary. If this is true, chemical substitutions and physical squeezing may be effective in placing $BaOsO_3$ into an unusual insulating state where the SO interaction is significant.

Finally, the crystal structure and magnetic and electrical properties of $BaOsO_3$ synthesized at a pressure of 17 GPa were investigated by SXRD analyses. The χ, ρ, and C_p values of the synthesized compound were also measured. Thus, a series of d^4 cubic perovskite oxides was established, which mapped out the evolution of itinerant ferromagnetism that was free from any complications from local lattice distortions for a transition from over the 3d orbital to the 5d orbital. Such a perovskite series has not been achieved at any d configuration to date. The $5d^4$ cubic $BaOsO_3$ exhibited enhanced paramagnetism to 2 K, while the d^4 cubic $BaFeO_3$ and $BaRuO_3$ were found to be itinerantly ferromagnetic at temperatures of 111 and 60 K, respectively. Cubic $BaOsO_3$ is possibly a nearly ferromagnetic metal rather than a paramagnetic metal, although it does not show a magnetically long-range order,[61,62] as evidenced by its high χ values greater than the expected Pauli paramagnetic suscept-

dx.doi.org/10.1021/ja4074408 | J. Am. Chem. Soc. 2013, 135, 16507−16516

ibility and owing to the fact that its γ value is greater than the expected value from the DOS at E_F. In addition, its DOS structure was indicative of magnetic instabilities. The SO interaction of the $5d^4$ electrons should be stronger than those of the $3d^4$ and $4d^4$ ones; however, establishing an unusual insulating state in which the SO interaction plays a significant role is not sufficient. Therefore, the *jj* coupling does not adequately describe all the properties of $BaOsO_3$. Further theoretical and quantitative studies of the SO interaction, *U*, and *W* in cubic perovskite $BaOsO_3$ are needed for characterizing the ferromagnetic evolution from 3d to 5d in group 8 elements. It should be noted that the local lattice distortion introduced in orthorhombic $SrOsO_3$ and $CaOsO_3$ did not markedly alter their magnetic properties, in contrast to the comparable orthorhombic/tetragonal Ru and Fe perovskite oxides. It is possible that an isoelectric compound with reduced structural dimensionality, such as layered Ba_2OsO_4, would lie on the boundary between metallic and unusually gapped states, if it is synthesized.

■ ASSOCIATED CONTENT

Ⓢ Supporting Information

Comparison of the lattice and structural parameters of the perovskite oxides. This material is available free of charge via the Internet at http://pubs.acs.org.

■ AUTHOR INFORMATION

Corresponding Authors

yangfeng.guo@physics.ox.ac.uk
yamaura.kazunari@nims.go.jp

Present Addresses

★Y. Guo: Condensed Matter Physics, Clarendon Laboratory, University of Oxford, Parks Road, Oxford OX1 3PU, United Kingdom.
⬠Y. Shirako: Texas Materials Institute, Cockrell School of Engineering, The University of Texas at Austin, 1 University Station C2201, Austin, TX 78712, USA.

Author Contributions

⬡Y. Shi and Y. Guo contributed equally.

Notes

The authors declare no competing financial interest.

■ ACKNOWLEDGMENTS

This research was supported in part by the World Premier International Research Center of the Ministry of Education, Culture, Sports, Science and Technology (MEXT), Japan, by the Japan Society for the Promotion of Science (JSPS) through a Grant-in-Aid for Scientific Research (Nos. 22246083, 25289233, 22340163, and 25287145), by the Funding Program for World-Leading Innovative R&D on Science and Technology (FIRST Program), Japan, and by the Ministry of Science and Technology of China (973 Project Nos. 2011CB921701 and 2011CBA00110). The authors thank the staff of BL15XU, the National Institute for Materials Science (NIMS), and SPring-8 for their help with the use of the beamline. The SXRD measurements were performed with the approval of the NIMS beamline station (Proposal Nos. 2011B4514, 2012B4506, and 2013A4504).

■ REFERENCES

(1) Liu, X.; Katukuri, V. M.; Hozoi, L.; Yin, W. G.; Dean, M. P. M.; Upton, M. H.; Kim, J.; Casa, D.; Said, A.; Gog, T.; Qi, T. F.; Cao, G.; Tsvelik, A. M.; van den Brink, J.; Hill, J. P. *Phys. Rev. Lett.* **2012**, *109*, No. 157401.
(2) Kim, J. W.; Choi, Y.; Kim, J.; Mitchell, J. F.; Jackeli, G.; Daghofer, M.; van den Brink, J.; Khaliullin, G.; Kim, B. J. *Phys. Rev. Lett.* **2012**, *109*, No. 037204.
(3) Arita, R.; Kunes, J.; Kozhevnikov, A. V.; Eguiluz, A. G.; Imada, M. *Phys. Rev. Lett.* **2012**, *108*, No. 086403.
(4) Kim, B. J.; Ohsumi, H.; Komesu, T.; Sakai, S.; Morita, T.; Takagi, H.; Arima, T. *Science* **2009**, *323*, 1329.
(5) Katsnelson, M. I.; Irkhin, V. Y.; Chioncel, L.; Lichtenstein, A. I.; de Groot, R. A. *Rev. Mod. Phys.* **2008**, *80*, 315.
(6) Norman, M. R.; Pines, D.; Kallin, C. *Adv. Phys.* **2005**, *54*, 715.
(7) Salamon, M. B.; Jaime, M. *Rev. Mod. Phys.* **2001**, *73*, 583.
(8) Imada, M.; Fujimori, A.; Tokura, Y. *Rev. Mod. Phys.* **1998**, *70*, 1039.
(9) Dagotto, E. *Rev. Mod. Phys.* **1994**, *66*, 763.
(10) Fung, H. K.; Williamson, S. J.; Ting, C. S. *Phys. Rev. B* **1975**, *11*, 2053.
(11) Haken, H.; Wolf, H. C. *The Physics of Atoms and Quanta: Introduction to Experiments and Theory*; Springerr-Verlag: Berlin Heidelberg, 2005.
(12) Calder, S.; Garlea, V. O.; McMorrow, D. F.; Lumsden, M. D.; Stone, M. B.; Lang, J. C.; Kim, J. W.; Schlueter, J. A.; Shi, Y. G.; Yamaura, K.; Sun, Y. S.; Tsujimoto, Y.; Christianson, A. D. *Phys. Rev. Lett.* **2012**, *108*, No. 257209.
(13) Du, Y. P.; Wan, X. G.; Sheng, L.; Dong, J. M.; Savrasov, S. Y. *Phys. Rev. B* **2012**, *85*, No. 174424.
(14) Jung, M. C.; Song, Y. J.; Lee, K. W.; Pickett, W. E. *Phys. Rev. B* **2013**, *87*, No. 115119.
(15) Shi, Y. G.; Guo, Y. F.; Yu, S.; Arai, M.; Belik, A. A.; Sato, A.; Yamaura, K.; Takayama-Muromachi, E.; Tian, H. F.; Yang, H. X.; Li, J. Q.; Varga, T.; Mitchell, J. F.; Okamoto, S. *Phys. Rev. B* **2009**, *80*, No. 161104.
(16) Cava, R. J.; Santoro, A.; Murphy, D. W.; Zahurak, S.; Roth, R. S. *J. Solid State Chem.* **1982**, *42*, 251.
(17) Mikhailova, D.; Ehrenberg, H.; Fuess, H. *J. Solid State Chem.* **2006**, *179*, 3672.
(18) Shi, Y. G.; Guo, Y. F.; Yu, S.; Arai, M.; Belik, A. A.; Sato, A.; Yamaura, K.; Takayama-Muromachi, E.; Varga, T.; Mitchell, J. F. *J. Solid State Chem.* **2010**, *183*, 402.
(19) Bremholm, M.; Dutton, S. E.; Stephens, P. W.; Cava, R. J. *J. Solid State Chem.* **2011**, *184*, 601.
(20) Okamoto, Y.; Nohara, M.; Aruga-Katori, H.; Takagi, H. *Phys. Rev. Lett.* **2007**, *99*, No. 137207.
(21) Pesin, D.; Balents, L. *Nat. Phys.* **2010**, *6*, 376.
(22) Matsuura, H.; Miyake, K. *J. Phys. Soc. Jpn.* **2013**, *82*, No. 073703.
(23) Dann, S. E.; Weller, M. T.; Currie, D. B. *J. Solid State Chem.* **1991**, *92*, 237.
(24) Mackenzie, A. P.; Maeno, Y. *Rev. Mod. Phys.* **2003**, *75*, 657.
(25) Matsuno, J.; Okimoto, Y.; Fang, Z.; Yu, X. Z.; Matsui, Y.; Nagaosa, N.; Kawasaki, M.; Tokura, Y. *Phys. Rev. Lett.* **2004**, *93*, No. 167202.
(26) Hase, I.; Nishihara, Y. *J. Phys. Soc. Jpn.* **1996**, *65*, 3957.
(27) Bocquet, A. E.; Fujimori, A.; Mizokawa, T.; Saitoh, T.; Namatame, H.; Suga, S.; Kimizuka, N.; Takeda, Y.; Takano, M. *Phys. Rev. B* **1992**, *45*, 1561.
(28) Cao, G.; McCall, S.; Shepard, M.; Crow, J. E.; Guertin, R. P. *Phys. Rev. B* **1997**, *56*, 321.
(29) Sarkozy, R. F.; Chamberland, B. L. *Mater. Res. Bull.* **1973**, *8*, 1351.
(30) Chamberland, B. L. *Mater. Res. Bull.* **1978**, *13*, 1273.
(31) Potze, R. H.; Sawatzky, G. A.; Abbate, M. *Phys. Rev. B* **1995**, *51*, 11501.
(32) Yamaura, K.; Takayama-Muromachi, E. *Phys. Rev. B* **2001**, *64*, No. 224424.
(33) Cao, G.; Durairaj, V.; Chikara, S.; DeLong, L. E.; Parkin, S.; Schlottmann, P. *Phys. Rev. B* **2007**, *76*, No. 100402.
(34) Li, Z.; Iitaka, T.; Tohyama, T. *Phys. Rev. B* **2012**, *86*, No. 094422.

(35) Zhou, J. S.; Matsubayashi, K.; Uwatoko, Y.; Jin, C. Q.; Cheng, J. G.; Goodenough, J. B.; Liu, Q. Q.; Katsura, T.; Shatskiy, A.; Ito, E. *Phys. Rev. Lett.* **2008**, *101*, No. 077206.
(36) Shirako, Y.; Satsukawa, H.; Wang, X. X.; Li, J. J.; Guo, Y. F.; Arai, M.; Yamaura, K.; Yoshida, M.; Kojitani, H.; Katsumata, T.; Inaguma, Y.; Hiraki, K.; Takahashi, T.; Akaogi, M. *Phys. Rev. B* **2011**, *83*, No. 174411.
(37) Tanaka, M.; Katsuya, Y.; Matsushita, Y.; Sakata, O. *J. Ceram. Soc. Jpn.* **2013**, *121*, 287.
(38) Tanaka, M.; Katsuya, Y.; Yamamoto, A. *Rev. Sci. Instrum.* **2008**, *79*, No. 075106.
(39) Izumi, F.; Momma, K. *Solid State Phenom.* **2007**, *130*, 15.
(40) Momma, K.; Izumi, F. *J. Appl. Crystallogr.* **2008**, *41*, 653.
(41) Perdew, J. P.; Burke, K.; Ernzerhof, M. *Phys. Rev. Lett.* **1996**, *77*, 3865.
(42) Blaha, P.; Schwarz, K.; Madsen, G. K. H.; Kvasnicka, D.; Luitz, J. *WIEN2K: An Augmented Plane Wave+Local orbitals Program for Calculating Crystal Properties*; Karlheinz Schwarz, Tech. Universitat Wien: Wien, Austria, 2001.
(43) Howard, C. J.; Stokes, H. T. *Acta Crystallogr.* **1998**, *B54*, 782.
(44) Glazer, A. M. *Acta Crystallogr.* **1972**, *B28*, 3384.
(45) Galoshina, E. V.; Gorina, N. B.; Polyakova, V. P.; Savitskii, E. M.; Shchegolikhina, N. I.; Volkenshtein, N. V. *Phys. Status Solidi B* **1973**, *58*, K45.
(46) Zheng, P.; Shi, Y. G.; Wu, Q. S.; Xu, G.; Dong, T.; Chen, Z. G.; Yuan, R. H.; Cheng, B.; Yamaura, K.; Luo, J. L.; Wang, N. L. *Phys. Rev. B* **2012**, *86*, No. 195108.
(47) O'Keeffe, M.; Hyde, B. *Acta Crystallogr.* **1977**, *B33*, 3802.
(48) Brown, I. D. *Chem. Rev.* **2009**, *109*, 6858.
(49) Jin, C. Q.; Zhou, J. S.; Goodenough, J. B.; Liu, Q. Q.; Zhao, J. G.; Yang, L. X.; Yu, Y.; Yu, R. C.; Katsura, T.; Shatskiy, A.; Ito, E. *Proc. Natl. Acad. Sci. U. S. A.* **2008**, *105*, 7115.
(50) Hayashi, N.; Yamamoto, T.; Kageyama, H.; Nishi, M.; Watanabe, Y.; Kawakami, T.; Matsushita, Y.; Fujimori, A.; Takano, M. *Angew. Chem., Int. Ed.* **2011**, *50*, 12547.
(51) Davies, P. K.; Wu, H.; Borisevich, A. Y.; Molodetsky, I. E.; Farber. *Annu. Rev. Mater. Res.* **2008**, *38*, 369.
(52) Hussey, N. E.; Takenaka, K.; Takagi, H. *Philos. Mag.* **2004**, *84*, 2847.
(53) Mott, N. F. *Philos. Mag.* **1970**, *22*, 7.
(54) Cheng, J. G.; Alonso, J. A.; Suard, E.; Zhou, J. S.; Goodenough, J. B. *J. Am. Chem. Soc.* **2009**, *131*, 7461.
(55) Goodenough, J. B.; Zhou, J. S. *Chem. Mater.* **1998**, *10*, 2980.
(56) Alexander, C. S.; Cao, G.; McCall, S.; Crow, J. E. *Jpn. J. Appl. Phys.* **1999**, *85*, 6223.
(57) Cheng, J.-G.; Zhou, J.-S.; Goodenough, J. B. *Proc. Natl. Acad. Sci. U. S. A.* **2013**, *110*, 13312.
(58) Lee, D. J.; Seo, Y. K.; Lee, Y. S.; Noh, H. J. *Solid State Commun.* **2010**, *150*, 301.
(59) Lee, Y. S.; Lee, J. S.; Noh, T. W.; Byun, D. Y.; Yoo, K. S.; Yamaura, K.; Takayama-Muromachi, E. *Phys. Rev. B* **2003**, *67*, No. 113101.
(60) Takano, M.; Nasu, S.; Abe, T.; Yamamoto, K.; Endo, S.; Takeda, Y.; Goodenough, J. B. *Phys. Rev. Lett.* **1991**, *67*, 3267.
(61) Yoshimura, K.; Imai, T.; Kiyama, T.; Thurber, K. R.; Hunt, A. W.; Kosuge, K. *Phys. Rev. Lett.* **1999**, *83*, 4397.
(62) He, T.; Cava, R. J. *Phys. Rev. B* **2001**, *63*, No. 172403.